ChinaRxiv

AI translation · View original & related papers at
chinarxiv.org/items/chinaxiv-201611.00290

Microstructure, Properties and Work Hardening Behavior of 1300 MPa Grade 0.14C-2.72Mn-1.3Si Steel (Postprint)

Authors: Zhao Zhengzhi, Tong Tingting, Zhao Aimin, He Qing, Dong Rui, Zhao Fuqing

Date: 2016-11-04T00:00:00+00:00

Abstract

On a continuous annealing simulator, an ultra-high-strength steel of the C-Si-Mn system (0.14C-1.3Si-2.72Mn) with Mn content intermediate between medium- and low-manganese levels was processed, yielding a multi-phase microstructure comprising ferrite, quenched martensite, tempered martensite, and a certain amount of retained austenite. Microstructural characterization of the experimental steel under different heat treatment conditions was performed using dilatometer, SEM, TEM, EBSD, XRD, and other techniques. The steel annealed at 800 ℃ exhibited optimal comprehensive mechanical properties, with a yield strength of 672 MPa, tensile strength of 1333 MPa, and total elongation of 13%. This is primarily attributed to the combined effects of the fine microstructure, appropriate phase proportions, and a certain amount of retained austenite in the 800 ℃ annealed steel. This paper presents an in-depth analysis of the work hardening behavior of the experimental steel, discussing the variation of its instantaneous n-value, employing the modified C-J method to analyze the multi-stage work hardening behavior, and investigating the influence of martensite structural parameters f/d, ferrite volume fraction, and other factors on work hardening. It is concluded that the high initial work hardening rate of the experimental steel originates from the proportion, morphology, and distribution of each phase, representing the result of coordinated interaction among the constituent phases and the synergistic action of multiple factors, which is beneficial for enhancing the strength and ductility-toughness of the experimental steel.

Full Text

Abstract

Multiphase microstructures containing ferrite, lath martensite, tempered martensite, and a specific proportion of retained austenite were produced in a C-Si-Mn series ultra-high strength steel with Mn content between low and medium levels (0.14C-1.3Si-2.72Mn, mass fraction, %) using a continuous annealing simulator. Microstructures of the steels under different heat treatment conditions were characterized by means of dilatometric simulation, SEM, TEM, EBSD, and XRD. The results demonstrate that the steel annealed at 800 °C achieved optimal comprehensive mechanical properties, with a yield strength of 672 MPa, tensile strength of 1333 MPa, and total elongation of 13%. This performance can be attributed to the refined microstructure, appropriate phase proportions, and a specific amount of retained austenite. The work hardening behavior of the experimental steel was thoroughly analyzed, including discussion of the instantaneous n-value (work hardening exponent) variation. Multi-stage work hardening behavior was investigated using a modified C-J method, exploring the influence of martensite structural parameters f/d (where f is the volume fraction of martensite and d is the equivalent diameter of martensite) and ferrite volume fraction on work hardening. The results show that prior to necking, n initially increases rapidly with true strain and then decreases, though the decreasing trend differs among steels annealed at different temperatures. Due to varying martensite volume fractions in steels annealed at different temperatures, the modified C-J analysis reveals two-stage and three-stage work hardening behaviors. The ferrite volume fraction significantly affects the strain range of plastic deformation under combined martensite and ferrite action: the co-deformation range is small at low temperatures, gradually increases at elevated temperatures, but may decrease again at excessively high temperatures. Overall, the high initial work hardening rate originates from the proportion, morphology, and distribution of each phase, resulting from coordinated deformation and combined effects of multiple factors, which is beneficial for improving the strength, ductility, and toughness of the steel.

Keywords: multiphase microstructure, retained austenite, work hardening behavior, uniform elongation, modified C-J analysis

Introduction

In recent years, domestic and foreign scholars have conducted in-depth research on advanced high-strength steels (AHSS), developing various grades including DP (Dual-phase) steel [**?**], TRIP (Transformation Induced Plasticity) steel [**?**, **?**], TWIP (Twinning Induced Plasticity) steel [**?**, **?**], and Q&P (Quenching and Partitioning) steel [**?**, **?**], which exhibit excellent comprehensive mechanical properties. Among these, Mn is a crucial element in ultra-high strength steels. Current research on Mn content in ultra-high strength steels primarily focuses on Mn 2.0% and Mn 4.0% (mass fraction) [**?**, **?**, **?**], with limited studies on the range

of 2.0%~4.0%. Zhong et al. [**?**] investigated the Q-P-T (Quenching-Partitioning-Tempering) process for a 0.2C-1.5Mn-1.5Si-0.05Nb-0.03Mo (mass fraction, %) high-strength steel, achieving a tensile strength of 1500 MPa and total elongation of 15%. However, the numerous alloying elements and strict process parameter control not only increase costs but also complicate microstructure control, making industrial production and application more difficult. Li et al. [**?**] studied the annealing process and microstructure evolution of a 0.08C-5Mn-0.15Si (mass fraction, %) medium-Mn hot-rolled TRIP steel, obtaining a tensile strength of 900 MPa and total elongation of 27%, but the tensile strength was relatively low. Moreover, DP and TRIP steels currently widely used in automotive applications generally have tensile strengths below 1000 MPa.

This work designed a C-Si-Mn series ultra-high strength steel with Mn content between medium and low levels, controlled within 2.0%~3.0%, without adding other alloying elements. Through a feasible industrial trial production scheme, the tensile strength of the experimental steel was increased to over 1300 MPa with a total elongation of 13%. The objective was to reduce costs, simplify the process, and enable automotive body applications. The microstructure morphology, phase composition, and mechanical properties of the experimental steel at different annealing temperatures were investigated, and the work hardening behavior at different deformation stages was thoroughly discussed. The effects of martensite structural parameters and phase proportions on work hardening behavior were also explored.

Experimental Procedures

The experimental steel was melted in a 50 kg medium-frequency vacuum induction furnace to produce an ingot, which was then forged into a 40 mm × 90 mm × 140 mm billet. The main chemical composition (mass fraction/%) was: C 0.14, Si 1.30, Mn 2.72, P 0.008, S 0.0037, with Fe balance. The forged billet was held at 1200 °C for 1 h, then hot-rolled through five passes to obtain a 4 mm thick hot-rolled sheet with a finishing temperature of 900 °C and a coiling temperature of 650 °C. After pickling, the hot-rolled sheet was cold-rolled with a reduction rate of 62.5% to obtain a 1.5 mm thick cold-rolled sheet. Annealing simulation of the cold-rolled sheet was performed on a ULVAC CCT-AY-steel sheet heat treatment simulator, with the specific process route shown in [FIGURE:1].

Rectangular specimens of 4 mm × 10 mm × 1.5 mm were cut from the cold-rolled sheet. Using a DIL 805A dilatometer and following the standard YB/T 5127-1993 "Method for Determining Critical Points of Steel (Dilatometric Method)," the phase transformation points of the experimental steel were measured. The Ac1 (temperature at which pearlite transforms to austenite during heating) and Ac3 (temperature at which all ferrite transforms to austenite in hypoeutectoid steel) were determined to be 699 °C and 843 °C, respectively, while Ms and Mf (start and finish temperatures of austenite-to-martensite transformation after austenitization and cooling) were 388 °C and 269 °C, respectively. Tensile spec-

imens with a gauge length of 50 mm and thickness of 1.5 mm were cut from the annealed sheets along the rolling direction. Tensile tests were conducted at room temperature at a strain rate of 2 mm/min, with two tests performed for each condition and average values reported.

Metallographic samples were polished and etched with 4% (volume fraction) nital solution, and microstructures were observed using a ZEISS ULTRA 55 field-emission scanning electron microscope (SEM). EBSD (Electron Backscattered Diffraction) specimens were cut from the annealed sheets, electropolished, and analyzed on a ZEISS ULTRA 55 field-emission SEM equipped with an HKL system at an accelerating voltage of 20 kV and step size of 0.2 m. Data acquisition was performed using HKL CHANNEL 5 software. Fine substructures of martensite and ferrite, as well as retained austenite distribution, were observed using a Tecnai G2 F30 S-TWIN transmission electron microscope (TEM). TEM specimens were prepared by twin-jet electropolishing using a 5% (volume fraction) perchloric acid alcohol solution cooled to -20 °C with liquid nitrogen at a voltage of 20-30 V.

Retained austenite in the experimental steel was measured using a D/MAX-RB X-ray diffractometer (XRD) with the following parameters: Cu target, 40 kV, 150 mA, step width of 0.02°, and scanning speed of 1 °/min. Step scanning was performed on three -phase diffraction lines (200) , (220) , (311) and two -phase diffraction lines (200) , (211) to accurately determine the corresponding diffraction angles 2 and integrated intensities I. The volume fraction of retained austenite was calculated using the direct comparison method [**?**]. The carbon content in retained austenite was then calculated using the following equation [**?**]:

$$C_\gamma = \frac{(a_\gamma - 0.3547)}{0.00467}$$

where C_γ is the mass fraction of carbon in retained austenite (%) and a_γ is the lattice constant of retained austenite (nm).

2.1 Effect of Annealing Temperature on Microstructure

SEM images of the microstructure of the annealed experimental steel are shown in [FIGURE:2], with volume fractions of different phases presented in . The microstructure primarily consists of ferrite and martensite. With increasing annealing temperature, the ferrite volume fraction decreases while the martensite volume fraction increases, and the martensite morphology becomes more diverse. On one hand, martensite blocks gradually coarsen, which depends on the size of austenite grains formed in the two-phase region. During low-temperature annealing, austenite nucleates at ferrite grain boundaries but grows slowly, resulting in fine austenite grains. At high annealing temperature, austenite nuclei gradually expand into ferrite interiors, leading to larger grain sizes. The mor-

phological changes in martensite are mainly related to the martensite transformation temperature range.

As shown in [FIGURE:2(a)], after annealing at 760 °C, the martensite is basically in an island-like quenched state, surrounded by bright white rims with gray centers. This phenomenon satisfies the kinetic model for austenite formation in the two-phase region proposed by Speich et al. [**?**]: the first step is controlled by carbon diffusion with short diffusion distances and rapid growth rates; the second step is controlled by manganese diffusion in ferrite, where Mn diffusion rate in ferrite is nearly three orders of magnitude higher than in austenite. Mn diffusion through or along ferrite grain boundaries leads to the formation of high-Mn rims around austenite nuclei, giving the rims higher hardenability than the cores, which results in the formation of bright martensite rims during cooling. During annealing at 760 °C, elements such as C and Mn diffuse into austenite nuclei, ultimately producing fine austenite enriched in C and Mn. The Ms temperature of this austenite may be below 240 °C. When the experimental steel is rapidly cooled to 240 °C, only a small portion of the austenite formed in the two-phase region transforms, with the remainder transforming to martensite during continued cooling to room temperature [**?**, **?**].

With increasing annealing temperature, the volume fraction of austenite formed in the two-phase region increases while its average carbon content decreases, reducing its stability. The Ms temperature of austenite gradually rises above 240 °C, and more martensite transforms during rapid cooling to 240 °C. This portion of martensite undergoes tempering to some extent during isothermal holding at 240 °C [**?**, **?**], destroying the martensite lath structure and blurring the edges. At an annealing temperature of 820 °C, which is close to the fully austenitic region, the Mf temperature of austenite approaches 269 °C. When rapidly cooled to 240 °C, the austenite has essentially completely transformed to martensite, which then undergoes tempering during isothermal holding. As shown in [FIGURE:2(d)], the microstructure consists primarily of uniform tempered martensite with only a small amount of ferrite.

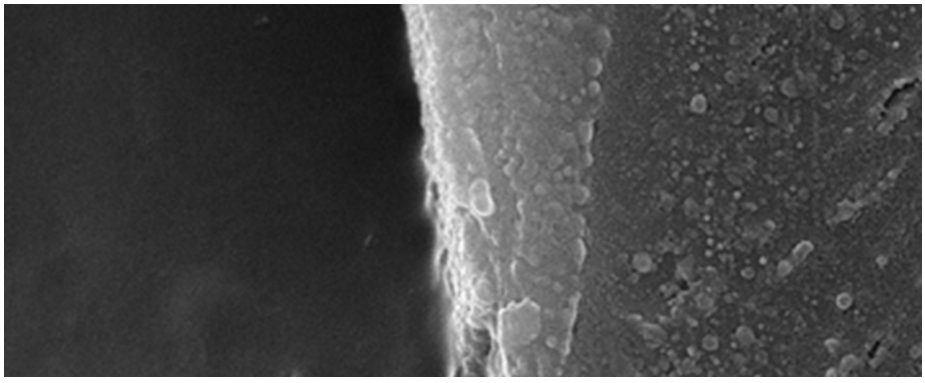

Figure 1: Figure 3

shows TEM images of martensite in specimens annealed at 760 and 800 °C. The images reveal differences in martensite block size and internal structure at different annealing temperatures. After annealing at 760 °C, the martensite blocks are fine with clear laths, characteristic of hardened martensite. At 800 °C, the martensite blocks are coarse with blurred lath boundaries, characteristic of tempered martensite, consistent with the above description.

2.2 Effect of Annealing Temperature on Mechanical Properties

[FIGURE:4] and

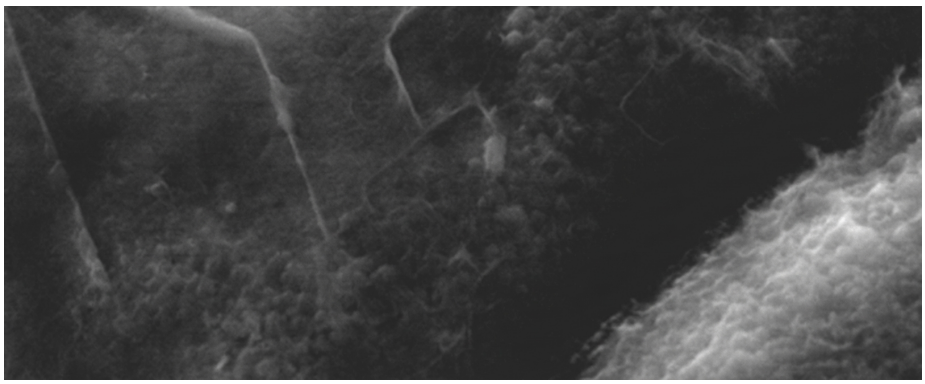

Figure 2: Figure 5

show the mechanical properties and stress-strain curves of the experimental steel annealed at different temperatures, respectively. As shown in [FIGURE:4], the tensile strength initially increases and then slightly decreases with increasing annealing temperature. This occurs because the austenite volume fraction increases with temperature, leading to a larger volume fraction of the hardening martensite phase upon cooling. Subsequently, the increased volume fraction of tempered martensite in the microstructure reduces dislocation density and weakens dislocation strengthening [**?**], offsetting the strengthening effect from increased martensite volume fraction.

The yield strength continuously increases with annealing temperature, primarily related to the ferrite volume fraction in the microstructure. During tensile deformation, the soft ferrite phase deforms first. As annealing temperature increases, the ferrite volume fraction decreases, reducing the initial total mobile dislocations in the microstructure and making yielding more difficult, thereby increasing the yield strength.

The total elongation initially increases and then decreases with annealing temperature. This is because, on one hand, the banding tendency weakens and ferrite becomes more uniformly refined with increasing temperature; on the

other hand, the degree of martensite recovery increases, accelerating the desaturation process of carbon atoms and reducing dislocation density and pile-up. The reduced total elongation after annealing at 820 °C is attributed to two factors: first, the decreased proportion of the soft ferrite phase; second, the coarsening of martensite blocks, which reduces the relative interfacial area and prevents stress concentration relief, decreasing the uniform deformation range under external stress.

As shown in

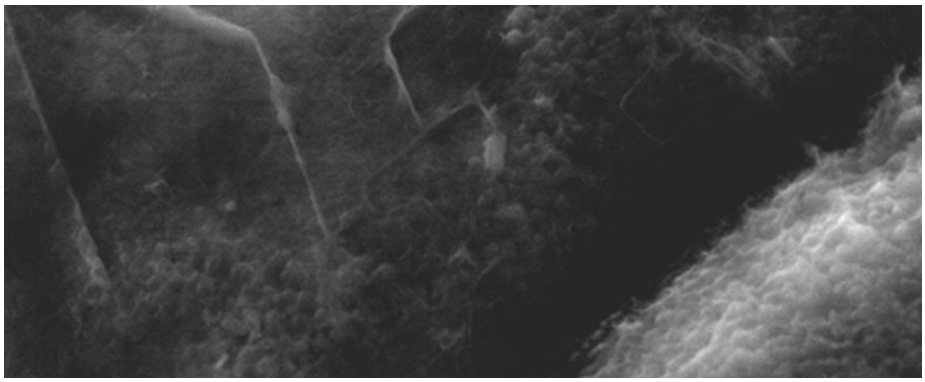

Figure 3: Figure 5

, the engineering stress-strain curves of the experimental steel exhibit no obvious yield plateau but rather continuous yielding. This results from volume expansion during martensite transformation during cooling, which exerts compressive stress on the surrounding microstructure equivalent to pre-deformation, reducing the process of interstitial atom pinning and unpinning during tensile deformation [**?**].

shows the volume fraction of each constituent phase and carbon content in retained austenite of the tested steel under different annealing temperatures.

2.3 Measurement and Distribution of Retained Austenite

XRD spectra of the experimental steel annealed at different temperatures are shown in [FIGURE:6], while [FIGURE:7] displays the retained austenite content and its carbon content at different annealing temperatures. As shown, more retained austenite is present after annealing at 760 °C. Although less austenite forms in the low-temperature two-phase region, its high carbon content stabilizes this austenite, allowing most of it to be retained to the aging zone for partitioning and remain stable at room temperature. At 780 °C, the austenite formed in the two-phase region increases while its carbon content decreases, reducing its stability and resulting in less austenite retained for partitioning at room temperature. However, the retained austenite increases after annealing at

800 °C, primarily due to the effect of aging at 240 °C. More martensite forms during the rapid cooling stage after annealing at 800 °C, and carbon diffusion from this martensite to the untransformed austenite facilitates carbon diffusion, increasing the stability of this austenite and enabling it to remain stable during subsequent cooling, thus increasing room-temperature retained austenite. When the temperature rises to 820 °C, the austenite formed in the two-phase region is too abundant with low average carbon content, and transformation is essentially complete during the rapid cooling stage, leaving little retained austenite at room temperature. In summary, the retained austenite content at room temperature results from multiple combined factors.

[FIGURE:7] also shows that the carbon content in retained austenite increases with annealing temperature, indicating that the main influencing factor may be: as annealing temperature increases, more austenite forms in the two-phase region, more martensite forms during rapid cooling, and carbon diffusion from martensite to austenite during aging increases the carbon content in room-temperature retained austenite.

[FIGURE:8] shows TEM images of retained austenite in the experimental steel annealed at 800 °C. The retained austenite exists in two morphologies: one as blocky islands distributed within martensite blocks, as shown in [FIGURE:8(a)] and [FIGURE:8(b)] (the inset in [FIGURE:8(a)] shows the diffraction pattern indexed as face-centered cubic), and the other as thin films distributed between martensite laths, as shown in [FIGURE:8(c)]. This retained austenite undergoes martensitic transformation under stress, producing stress relaxation that delays crack initiation while simultaneously forming a hardening phase that increases tensile strength and provides continuous work hardening. This is one reason why the annealed experimental steel exhibits high strength and relatively good ductility [**?**].

3.1 Instantaneous n-value (Work Hardening Exponent)

Under uniform deformation conditions, the stress-strain relationship can be expressed as $\sigma = k\varepsilon^n$ (where σ is true stress, ε is true strain, k is the strength coefficient, and n is the work hardening exponent). Taking the logarithm of both sides gives $n = d(\ln\sigma)/d(\ln\varepsilon)$, which describes the work hardening behavior during deformation. According to calculation results [**?**], the uniform true strain at necking is numerically equal to the instantaneous n-value, which reaches its maximum when the uniform true strain peaks. The instantaneous n-value corresponds to the slope of the $\ln\sigma$-$\ln\varepsilon$ curve.

shows the relationship between n and ε for experimental steel annealed at 760-820 °C. The intersection of the curve with the line $n = \varepsilon$ represents the uniform true strain at which necking occurs. Converting this true strain to engineering strain yields the uniform elongation. As shown, necking occurs at $\varepsilon = 0.051$, 0.087, 0.078, and 0.084 for steels annealed at 760, 780, 800, and 820 °C, respectively. The trend of n variation with increasing ε before necking differs among

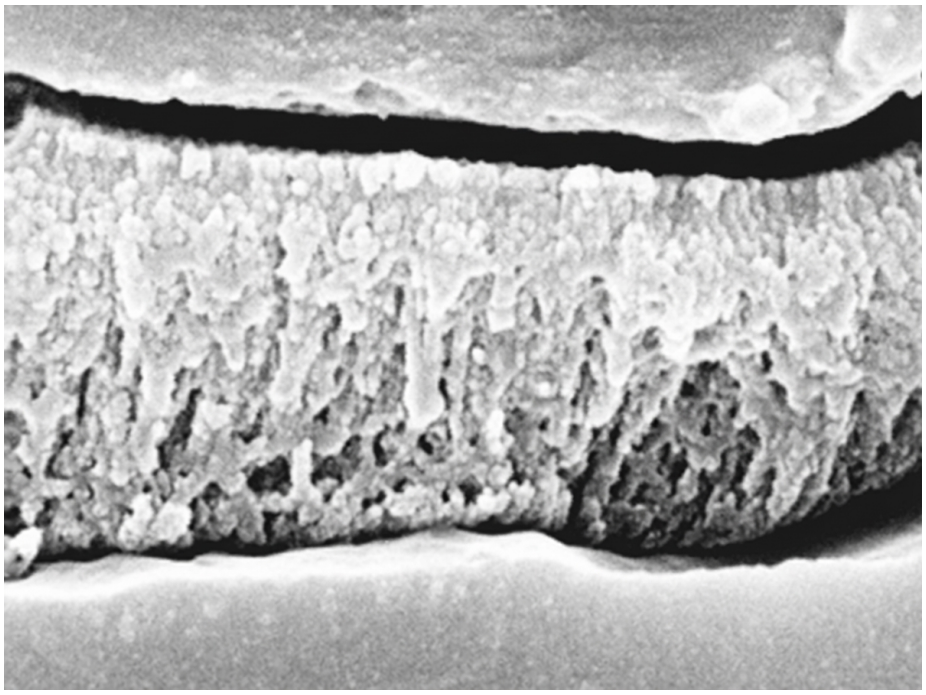

Figure 4: Figure 9

steels annealed at different temperatures. In the initial stage, n rapidly increases to a maximum value before quickly decreasing. When ε exceeds approximately 0.006, n slightly increases for the 760 °C annealed steel, while the decreasing rate of n significantly weakens for the 780 °C annealed steel, slightly weakens for the 800 °C annealed steel, and remains unchanged for the 820 °C annealed steel. When ε exceeds approximately 0.012, n decreases with increasing ε in all cases.

3.2 Multi-stage Work Hardening Behavior

High-strength steels often exhibit multi-stage work hardening characteristics. Research [**?**] has indicated that the Crussard-Jaoul method based on the modified Swift equation can reflect hardening mechanisms at different deformation stages, as shown in Equation (2):

$$\varepsilon = \varepsilon_0 + K\sigma^m \qquad (2)$$

where m and K represent the stress exponent and material constant, respectively, and ε_0 is the maximum elastic strain.

Equation (2) can be transformed as follows:

$$\sigma^{m-1} = \frac{1}{mK}\left(\frac{d\sigma}{d\varepsilon}\right) \qquad (3)$$

$$\ln\left(\frac{d\sigma}{d\varepsilon}\right) = (1-m)\ln\sigma - \ln(Km) \qquad (4)$$

Equation (4) shows that $\ln(d\sigma/d\varepsilon)$ varies linearly with $\ln\sigma$ with a slope of $(1-m)$, indicating that smaller m values correspond to greater work hardening rates. Nie et al. [**?**] found that for F/M dual-phase steels exhibiting continuous yielding during tensile testing, $\ln(d\sigma/d\varepsilon)$ versus $\ln\sigma$ generally exhibits three linear stages: initial uniform deformation of ferrite with elastic deformation of martensite; ferrite deformation constrained by martensite with elastic deformation of martensite; and combined plastic deformation of ferrite and martensite. If the martensite volume fraction is high, the first stage is replaced by the second stage, resulting in two-stage work hardening behavior.

[FIGURE:10] presents the analysis results of work hardening behavior using the modified C-J method, where m_{I}, m_{II}, and m_{III} represent the stress exponents at different stages. As shown, steels annealed at 760 and 780 °C with lower martensite volume fractions exhibit three linear stages, while steels annealed at 800 and 820 °C with higher martensite volume fractions show two linear stages. This is similar to results reported by Nie et al. [**?**] for dual-phase steels and demonstrates that the small amount of retained austenite in the experimental steel has minimal effect on work hardening.

From $\sigma = K\varepsilon^n$ and $\varepsilon = \varepsilon_0 + K\sigma^m$, it is evident that n and m are essentially equivalent before necking, with n equal to $1/m$. lists the stress exponents at different work hardening stages and the strain at transition points obtained from the modified C-J analysis. For the 760 °C annealed steel, the stress exponent relationship across three stages is: $1/m_{\mathrm{II}} > 1/m_{\mathrm{I}} > 1/m_{\mathrm{III}}$. For the 780 °C annealed steel: $1/m_{\mathrm{I}} > 1/m_{\mathrm{II}} > 1/m_{\mathrm{III}}$. For the 800 and 820 °C annealed steels with two stages: $1/m_{\mathrm{II}} > 1/m_{\mathrm{III}}$. This matches the overall trend of n variation with increasing ε shown in

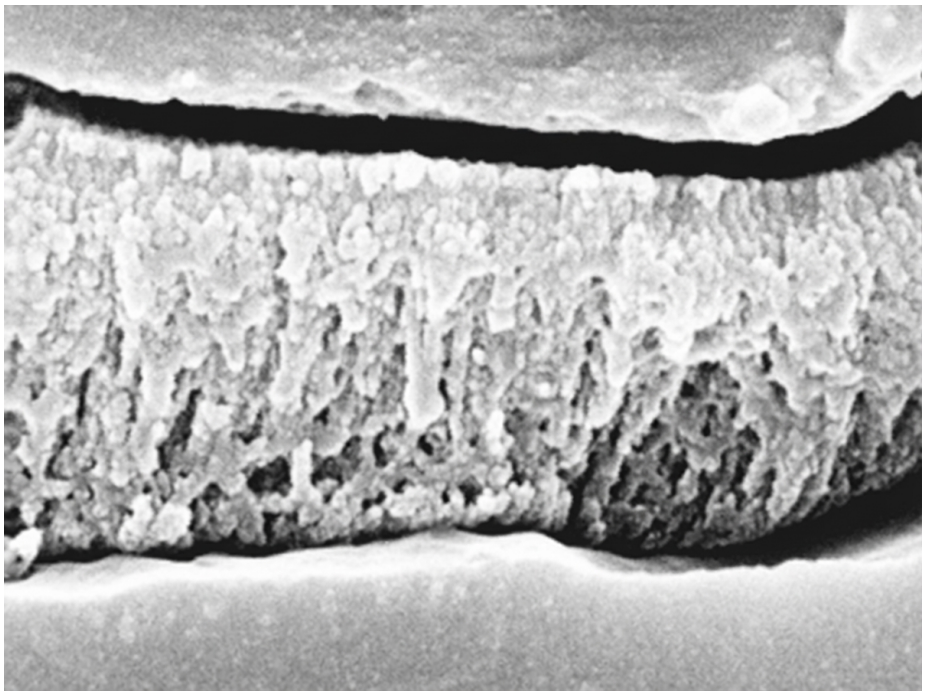

Figure 5: Figure 9

.

Combined analysis of

and reveals that for the 760 °C annealed steel, when $\varepsilon \leq 0.009$ (Stage I), deformation occurs primarily in ferrite. Under external stress, dislocation density in ferrite increases rapidly, causing dislocation pile-up and a rapid increase in flow stress, making n rise quickly. As strain increases, mobile dislocation density in the matrix increases, reducing deformation resistance and weakening work hardening, causing n to decrease rapidly. When $0.009 < \varepsilon < 0.018$ (Stage II), n increases rather than decreases, indicating enhanced work hardening that corresponds to $1/m_{\mathrm{II}} > 1/m_{\mathrm{I}}$ at 760 °C. This may be due to the large ferrite volume fraction at low annealing temperatures, which provides more mobile dislocations

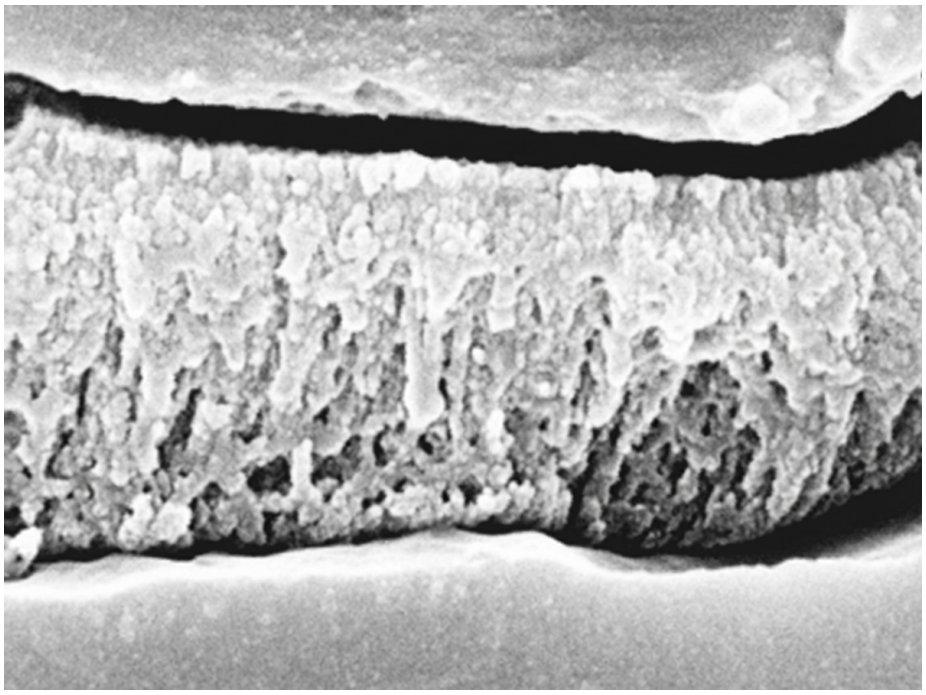

Figure 6: Figure 9

within ferrite. When $0.018 < \varepsilon < 0.051$ (Stage III), the combined plastic deformation of ferrite and martensite occurs, with n gradually decreasing and rapidly dropping in the later stage, significantly weakening work hardening. This may be related to the small martensite volume fraction after 760 °C annealing and poor coordination during combined action, corresponding to the smallest $1/m_{\mathrm{III}}$ at 760 °C. Similarly, for the 780 °C annealed steel, work hardening is highest in Stage I due to uniform ferrite deformation, moderately high in Stage II (differing from 760 °C due to ferrite/martensite ratio affecting stress transfer), and weakest in Stage III. For the 800 and 820 °C annealed steels with high martensite volume fractions, Stage I is replaced by Stage II, directly entering Stage II where work hardening is stronger overall than in Stage III.

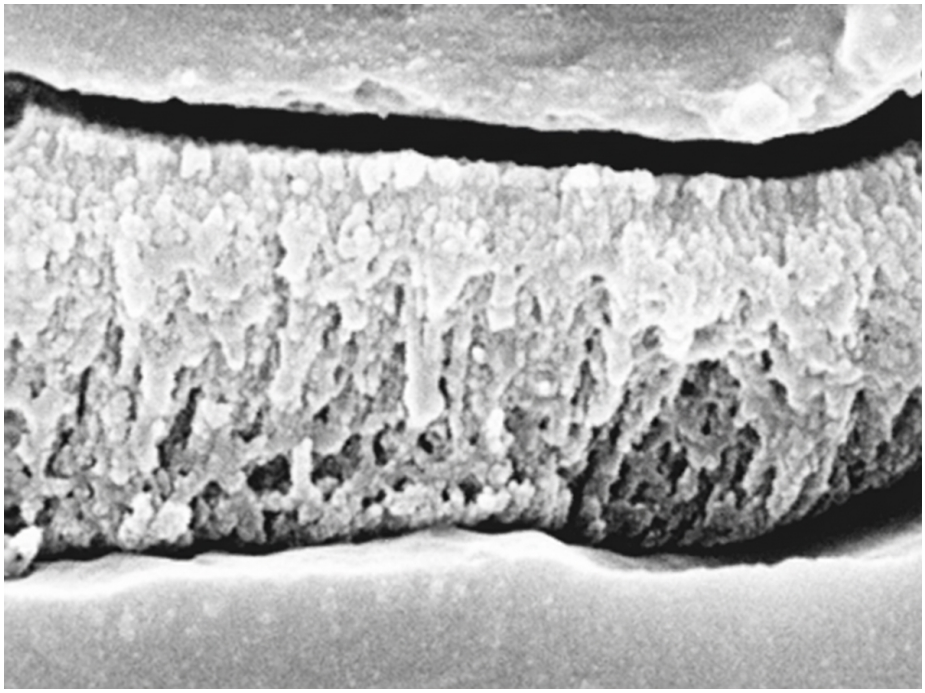

Figure 7: Figure 9

also shows that in Stage III, as annealing temperature increases, martensite volume fraction and block size increase, facilitating stress transfer and causing n to decrease rapidly. Moreover, higher annealing temperatures lead to more pronounced martensite tempering during aging, reducing dislocation density and deformation resistance, which also causes n to decrease [**?**].

3.3 Analysis of Microstructural Effects on Work Hardening Behavior

Research [**?**] has indicated that structural parameters such as ferrite grain size and volume fraction, as well as martensite morphology and distribution, significantly affect the tensile behavior of high-strength steels. The martensite volume fraction f directly influences stress transfer among phases during deformation, thereby affecting yield strength and work hardening behavior, while the average equivalent diameter d of martensite has the opposite effect [**?**, **?**]. This section focuses on the analysis of structural parameter f/d effects on work hardening behavior. EBSD technology was used to statistically determine the average equivalent grain sizes of ferrite (d_F) and martensite lath packets (d_M) in the annealed experimental steel, as shown in . In this work, boundaries with misorientation greater than 10° were defined as martensite packet boundaries. [FIGURE:11] shows orientation imaging maps of the experimental steel microstructure, clearly demonstrating that the prior austenite grains and martensite packets in the 760 °C annealed steel are finer than those in the 800 °C annealed steel. The d_M values were statistically determined using HKL CHANNEL 5 software and the following equation:

$$d_M = \sqrt{\frac{\sum_{i=1}^{N} S_i}{N}}$$

where S_i is the area of the ith martensite packet and N is the number of martensite packets.

Statistical results () show that the average equivalent grain sizes of martensite packets in steels annealed at different temperatures are 0.23, 0.51, 0.82, and 1.42 m, respectively. The numerous high-angle grain boundaries in fine martensite packets can increase crack propagation resistance and effectively hinder crack growth. also presents the martensite f/d parameter along with extreme n values ($n_{\max}$ and $n_{\min}$) and ($n_{\max}-n_{\min}$), where $n_{\min}$ and $n_{\max}$ represent the minimum starting point and maximum peak n values in Stage I of

, respectively. As annealing temperature increases from 760 to 780 °C, f/d decreases from 11.07 to 7.04, $n_{\max}$ increases from 0.58 to 0.64, and $n_{\min}$ increases from 0.38 to 0.54. The f/d parameter has a greater influence on $n_{\min}$ than on $n_{\max}$, consistent with research findings [**?**]. Additionally, $(n_{\max} - n_{\min})$ decreases with increasing annealing temperature (i.e., decreasing f/d), indicating that f/d has a greater effect on $(n_{\max} - n_{\min})$ at low annealing temperatures, suggesting higher sensitivity of this factor in the low-temperature regime. This is because at lower annealing temperatures, larger f/d values indicate greater martensite dispersion, which increases mobile dislocation density in ferrite during martensite formation, thereby promoting work hardening and resulting in larger $(n_{\max} - n_{\min})$. Conversely, $(n_{\max} - n_{\min})$ becomes smaller.

[FIGURE:12] illustrates the relationship between the strain range ε of combined

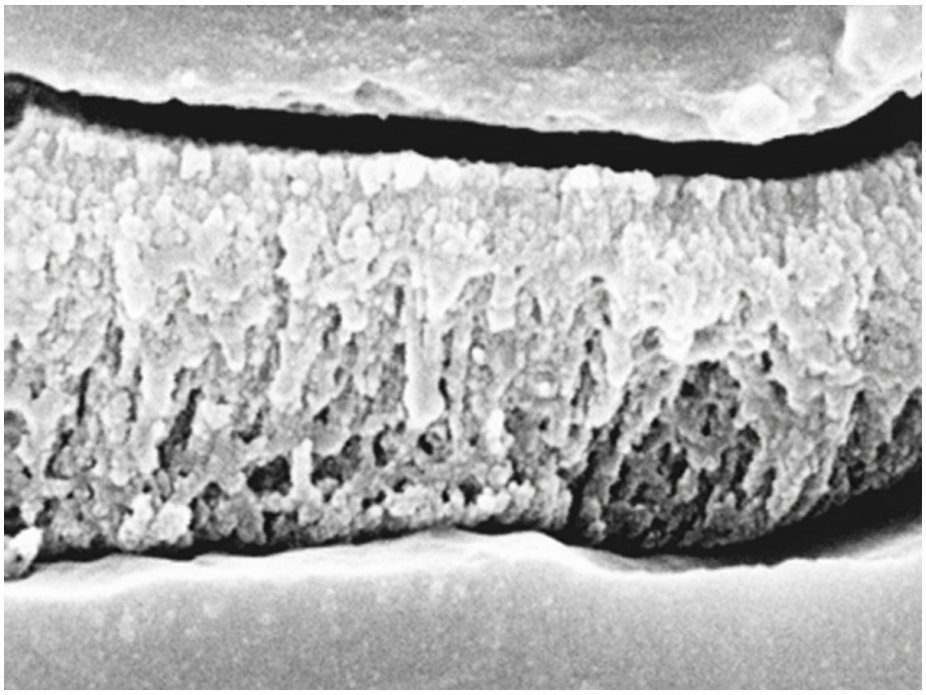

Figure 8: Figure 9

plastic deformation of martensite and ferrite (corresponding to the interval from the transition point between Stages II and III to the strain at necking in the C-J analysis) and the ferrite volume fraction f_F. Analysis using the modified C-J method indicates that the soft ferrite phase not only provides good ductility itself, increasing uniform elongation, but also extends the plastic deformation range of martensite [**?**]. As shown, when annealed at 760 °C, the experimental steel has excessive ferrite volume fraction, and the martensite is in a quenched state ([FIGURE:2(a)]), resulting in minimal stress transfer to martensite during deformation and a very small plastic deformation amount during combined martensite-ferrite action. When annealing temperature is 780-820 °C, ferrite volume fraction gradually decreases while martensite morphology changes from quenched to tempered, significantly increasing the strain range of combined plastic deformation. This occurs because stress is transferred from ferrite to martensite through the interface. On one hand, the presence of an appropriate proportion of soft ferrite phase slows down stress concentration in martensite. On the other hand, tempered martensite is more conducive to stress transfer. Therefore, the overall coordination of soft and hard phases enhances the strain range of combined plastic deformation of martensite and ferrite. The figure also shows that at higher annealing temperatures, the effect of ferrite volume fraction on the combined plastic deformation range becomes relatively stable. Based on this analysis, when ferrite volume fraction is very small, few mobile dislocations exist in ferrite, and ferrite may undergo plastic deformation before stress can be effectively transferred, likely causing the combined plastic deformation range to decrease again. This requires further experimental verification, as indicated by the dotted line in [FIGURE:12].

Conclusions

(1) The annealed 0.14C-2.72Mn-1.3Si steel microstructure consists of martensite, ferrite, and a small amount of retained austenite. The martensite is partially tempered, while retained austenite exists either as thin films between martensite laths or as blocky islands within martensite blocks.

(2) Optimal comprehensive mechanical properties are obtained after annealing at 800 °C: yield strength of 672 MPa, tensile strength of 1333 MPa, total elongation of 13%, yield ratio of 0.5, and strength-ductility product of 16.9 GPa · %. This performance is primarily attributed to the refined microstructure, appropriate phase proportions, and a certain amount of retained austenite.

(3) Prior to necking, n initially increases rapidly with true strain and then decreases, though the decreasing trend differs among steels annealed at different temperatures. Modified C-J analysis of multi-stage work hardening behavior reveals the following stress exponent relationships: for 760 °C annealed steel, $1/m_{\mathrm{II}} > 1/m_{\mathrm{I}} > 1/m_{\mathrm{III}}$; for 780 °C annealed steel, $1/m_{\mathrm{I}} > 1/m_{\mathrm{II}} > 1/m_{\mathrm{III}}$; and for 800 and 820 °C annealed steels, $1/m_{\mathrm{II}} > 1/m_{\mathrm{III}}$. These relationships match the overall trend of n varia-

tion with increasing ε.

(4) The martensite f/d parameter has a significant effect on $(n_{\max}-n_{\min})$ after low-temperature annealing. Ferrite volume fraction significantly affects the strain range $\Delta\varepsilon$ of combined plastic deformation of martensite and ferrite: the co-deformation range is small when ferrite volume fraction is too high at low temperatures, gradually increases at elevated temperatures, but may decrease again at excessively high temperatures.

References

[1] Hayami S, Furukawa T. Microalloying 75. New York: Union Carbide Corp, 1977: 311
[2] Matsumura O, Sakuma Y, Takechi H. Scr Metall, 1987; 21: 1301
[3] Sugimoto K, Misu M, Kobayashi M, Shirasawa H. ISIJ Int, 1993; 33: 775
[4] Bouaziz O, Guelton N. Mater Sci Eng, 2001; A319-321: 246
[5] Barnett M R. Mater Sci Eng, 2007; A464: 1
[6] Speer J G, Matlock D K, De Cooman B C, Schroth J G. Acta Mater, 2003; 51: 2611
[7] Matlock D K, Brautigam V E, Speer J G. Mater Sci Forum, 2003; 426-432: 1089
[8] Jiang H T, Tang D, Mi Z L, Chen Y L. J Univ Sci Technol Beijing, 2010, 32(2): 201
[9] Nouri A, Saghafian H, Kheirandish S. J Iron Steel Res, Int, 2010, 17(5): 44
[10] Fan Y, Wang M L, Zhang H, Tao H B, Zhao P, Li S Q. J Univ Sci Technol Beijing, 2013, 35(5): 607
[11] Zhong N, Wang X D, Wang L, Rong Y H. Mater Sci Eng A, 2009, 506(1): 111
[12] Li Z, Zhao A M, Tang D, Mi Z L, Jiao D H. J Univ Sci Technol Beijing, 2012, 34(2): 132
[13] Zhang L Y, Wu D, Li Z. J Iron Steel Res, Int. 2012; 19(2): 42
[14] Koh-ichi S, Daiki F, Nobuo Y. Pro Eng, 2010; 2: 359
[15] Speich G R, Demarest V A, Miller R L. J. Metal Trans A, 1981, 12(8): 1419
[16] Anazadeh A S, Sh.K. Mater Sci Eng A, 2012; 532: 21
[17] Rosenberga G, Sinaiováa I, Juhar Ľ. Mater Sci Eng A, 2013, 582: 347
[18] Yan S, Liu X H, Liu W J, Lan H F, Wu H Y. Acta Metall Sin, 2013; 49: 917
[19] Wang C Y, Shi J, Cao W Q, Dong H. Acta Metall Sin, 2011; 47: 720
[20] Mohammad R A, Ekrami A. Mater Sci Eng A, 2008, 477: 30
[21] Kang Y L, Kuang X, Yin X D. Auto Technol & Matel, 2006; 5: 1
[22] Ren Y Q, Xie Z J, Shang C J. Acta Metall Sin. 2012; 48: 1074
[23] Li Y L. J Chongqing Univ (Nat Sci), 2001; 24(3): 58
[24] Colla V, Sanctis D M, Dimatteo A. Metal Mater Trans. 2009; 40(11): 2557
[25] Nie W J, Shang C J, Guan H L, Zhang X B, Chen S H, Acta Metall Sin. 2012; 48: 298
[26] Zhao Z Z, Ye J Y, Wang Z Z, Zhao A M. J Shenyang Univ Technol. 2013;

35: 36
[27] Seyedrezai H, Pilkey A K, Boyd J D. Mater Sci Eng A, 2014; 594: 178
[28] Mazinani M, Poole W J. Metal Mater Trans. 2007; A38: 328
[29] Lanzillotto C A N, Pickering F B. Metal Sci. 1982; 16: 371
[30] Ashby M F. Philos Mag. 1966; 14: 1157
[31] Ashby M F. Philos Mag. 1970; 21: 399

Source: ChinaXiv —Machine translation. Verify with original.